DOI: 10.1002/chem.200501483

Probing the Transition between the Localised (Class II) and Localised-to-Delocalised (Class II–III) Regimes by Using Intervalence Charge-Transfer Solvatochromism in a Series of Mixed-Valence Dinuclear Ruthenium Complexes

Deanna M. D'Alessandro,[a] Amy C. Topley,[a, b] Murray S. Davies,[a] and F. Richard Keene*[a]

Abstract: Intervalence charge-transfer (IVCT) solvatochromism studies on the diastereoisomeric forms of $[\{Ru(bpy)_2\}_2(\mu\text{-BL})]^{5+}$ (bpy = 2,2′-bipyridine; BL = a series of di-bidentate polypyridyl bridging ligands) reveal that the solvent dependencies of the IVCT transitions decrease as the "tail" of the bridging ligand is extended, and the extent of delocalisation increases. Utilising a classical theoretical approach for the analysis of the intervalence charge-transfer (IVCT) solvatochromism data, the subtle and systematic variation in the electronic properties of the bridging ligands can be correlated with the shift between the localised (class II) and localised-to-delocalised (class II–III) regimes. The investigation of the diastereoisomeric forms of two series of complexes incorporating analogous structurally rigid (fused) and nonrigid (unfused) bridging ligands demonstrates that the differences in the IVCT characteristics of the diastereoisomers of a given complex are accentuated in the latter case, due to a stereochemically induced redox asymmetry contribution. The marked dependence of the IVCT transitions on the stereochemical identity of the complexes provides a quantitative measure of the fundamental contributions of the reorganisational energy and redox asymmetry to the intramolecular electron-transfer barrier at the molecular level.

Keywords: chirality · mixed-valent compounds · ruthenium · solvatochromism

Introduction

A pivotal problem in the analysis of mixed-valence complexes is the extent of electronic delocalisation between the metal centres, which is governed by competition between the electronic coupling (H_{ab}) and the sum of the Franck–Condon reorganisational energies (λ), the redox asymmetry (ΔE_0) and additional contributions due to spin–orbit coupling and ligand-field asymmetry ($\Delta E'$).[1,2] Classically, λ is partitioned into an inner-sphere vibrational component (λ_i), corresponding to the energy required for reorganisation of the metal–ligand and intraligand bond lengths and angles, and an outer-sphere component (λ_o), corresponding to the energy required for reorganisation of the surrounding solvent medium. According to Marcus–Hush theory,[1–4] these fundamental parameters govern the activation barrier to intramolecular electron transfer, and may be assessed by probing the characteristics of the IVCT transitions—specifically, their energy (ν_{max}), intensity (ε_{max}) and bandwidths ($\Delta\nu_{1/2}$)—observed in dinuclear mixed-valence complexes. In weakly coupled systems, the energy of the IVCT band is given by Equation (1):[1,2]

$$\nu_{max} = \lambda_i + \lambda_o + \Delta E_0 + \Delta E' \quad (1)$$

The degree of delocalisation, and the classification of mixed-valence systems within the Robin and Day scheme[5] is dependent on the relative magnitudes of H_{ab} and the sum of the factors that govern the activation barrier to electron transfer in Equation (1): "localised" class II systems are distinguished by weakly coupled centres ($2H_{ab} \ll \lambda$) and "delo-

[a] Dr. D. M. D'Alessandro, A. C. Topley, Dr. M. S. Davies, Prof. F. R. Keene
School of Pharmacy and Molecular Sciences
James Cook University, Townsville, Queensland 4811 (Australia)
Fax: (+61) 7-4781-6078
E-mail: Richard.Keene@jcu.edu.au

[b] A. C. Topley
Department of Chemistry, University of Southampton
Highfield, Southampton SO17 1BJ (UK)

Supporting information for this article is available on the WWW under http://www.chemeurj.org/ or from the author.

calised" class III systems by strongly coupled centres ($2H_{ab} \gg \lambda$). Experimentally, the classification of mixed-valence complexes is generally based upon the solvent dependence and observed bandwidth at half-height.[1,2] In localised systems, the IVCT bands are of low intensity and broad ($\varepsilon_{max} \leq 5000\,M^{-1}cm^{-1}$, $\Delta\nu_{1/2} \geq 2000\,cm^{-1}$) due to coupling with solvent. In delocalised species, the bands arise from transitions within the molecular orbital manifold of the systems and the bands are intense, narrow ($\varepsilon_{max} \geq 5000\,M^{-1}cm^{-1}$, $\Delta\nu_{1/2} \leq 2000\,cm^{-1}$) and solvent-independent.

The elucidation of the factors that govern the localised-to-delocalised transition in mixed-valence systems is complicated by the interplay between the timescales for intramolecular electron transfer and the coupled nuclear and solvent vibrations. A recent seminal review by Meyer and co-workers[6] addressed these issues from a semiclassical perspective, by defining mixed-valence systems in the localised-to-delocalised transition as "class II–III" ($2H_{ab} \approx \lambda$). This classification poses a further complexity as two transition regions—between classes II and II-III, and between classes II-III and III—are additionally required.

The distinction between the various classes is based on the dynamic characteristics of the systems and the relative timescales of the solvent, vibrational and electronic motions.[6,7] The lower-frequency solvent modes are treated classically, while the collective higher-frequency, inner-shell vibrations are treated quantum mechanically (i.e., $\lambda = \lambda_o + \Sigma\lambda_i$). As H_{ab} increases in a closely related series of complexes, the barrier to electron transfer decreases, as does the timescale for this process. If the solvent barrier is initially eliminated ($\lambda_o < \Sigma\lambda_i$), then the solvent modes for the donor and acceptor sites are averaged in the region in which $\lambda_o < 2H_{ab} < \lambda_o + \Sigma\lambda_i$. However, the two sites remain structurally distinct and will exhibit localised oxidation states. This scenario occurs if the rate of electron transfer (k_{et}) is intermediate between the frequencies for solvent reorientations (10^{11}–$10^{12}\,s^{-1}$) and bond vibrations (10^{13}–$10^{14}\,s^{-1}$), such that $k_{et} \sim 10^{12}$–$10^{13}\,s^{-1}$ and $0.7 < 2H_{ab}/\lambda < 1$. On this basis, operational definitions[6] for the various classes have been proposed: in class II the solvent and exchanging electron are localised; in class II–III the solvent modes are averaged, but the exchanging electron is localised; and in class III, the exchanging electron is delocalised and the solvent and vibrational modes are averaged. Although a system is considered to be fully delocalised when $2H_{ab} \gg \lambda$, the effects of transient charge localisation may still be observed on the IR timescale for a borderline class III system.[6,7]

In reality, the transitions between the regimes are not abrupt, and experimental studies have revealed a gradation in behaviour between the fully localised (class II) and fully delocalised (class III) limits that is governed by the relative timescales for intramolecular electron transfer and multiple nuclear and solvent vibrations coupled to the electron transfer.[6] The description is further challenged experimentally by the appearance of multiple IVCT and IC (interconfigurational) transitions in transition-metal-containing chromophores, in addition to contributions from environmental effects such as specific solvation and ion-pairing.[8]

While the classification of mixed-valence systems is not straightforward and relies on observations from several experimental techniques with widely different timescales,[6] the appearance of IVCT bands and their solvent dependence provides the most useful experimental criterion for distinguishing between classes II (broad, solvent-dependent, localised oxidation states) and II–III (narrow, solvent-independent, localised oxidation states). Due to the limited number of experimental studies in which the intricacies in behaviour in the localised-to-delocalised transition have been systematically explored, there is currently extensive interest in the elucidation of the fundamental factors that govern the transition.[6,7,9–11]

Recent studies in our laboratory have demonstrated that the diastereoisomers of symmetrical dinuclear mixed-valence complexes of the form $[\{M(pp)_2\}_2(\mu\text{-}BL)]^{5+}$ (M = Ru, Os; pp = a symmetrical polypyridyl bidentate ligand such as 2,2′-bipyridine (bpy); BL = a di-bidentate polypyridyl bridging ligand such as those shown here) provide subtle and systematic probes to examine the microscopic origins of the factors that govern the electron transfer barrier in Equation (1). These include solvent reorganisational contributions,[12] ion-pairing and temperature effects,[13] redox asymmetry contributions due to stereochemically induced structural distortions[14,15] and spin–orbit coupling contributions,[16] which are manifested by different electrochemical and IVCT properties for the diastereoisomeric forms of the same complex.

While the identity and coordination environments of the metal centres are identical in each diastereoisomeric form, a significant difference may be discerned in the nature of the "clefts" formed between the planes of the terminal bpy li-

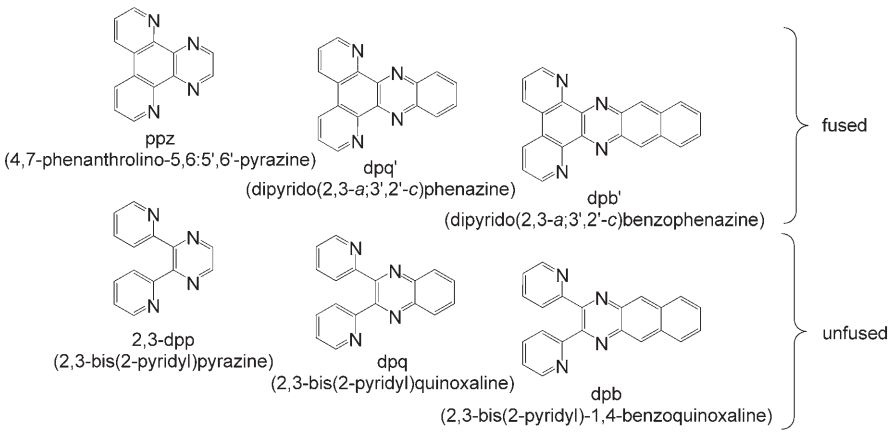

gands.[17] Interior clefts are formed between the bpy ligands immediately above and below the plane of the bridging ligand, and are approximately parallel in the *meso* ($\Lambda\Delta \equiv \Delta\Lambda$) form and approximately orthogonal in the *rac* ($\Delta\Delta/\Lambda\Lambda$) form, as shown in Figure 1.[17,18] In addition, exterior clefts are evident between the planes of the terminal bpy ligands at either end of the complex, and are identical for two diastereoisomeric forms.

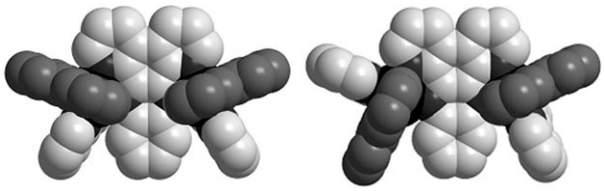

Figure 1. Chem3D representations (view from above the plane of the bridging ligand) of the *meso* ($\Lambda\Delta$) and *rac* ($\Delta\Delta$) diastereoisomers of $[\{Ru(bpy)_2\}_2(\mu\text{-dpq}')]^{4+}$. The bpy ligands above the plane of the bridge are highlighted to show the different dimensions of the clefts in the two forms.

The variation in the dimensions of the clefts between the diastereoisomeric forms of the same complex may have significant consequences for differential solvent and anion association at the molecular level. Indeed, the differential association of eluent anions such as toluene-4-sulfonate ($[CH_3(C_6H_4)SO_3]^-$) gives rise to the separation of the diastereoisomeric forms in the chromatographic cation-exchange separation process.[17–20]

The diastereoisomers exhibit several attractive features over dinuclear complexes that have been employed to date for IVCT studies: 1) the complexes are structurally rigid and 2) the dimensions of the clefts may be systematically modified through stereochemical variation, bridging ligand modification, or the judicious positioning of substituents on the terminal polypyridyl ligands, while maintaining the identity and coordination environments of the component metal centres. A further important feature is the extensive tuning of the ground-state electronic properties of the mixed-valence complexes $[\{Ru(bpy)_2\}_2(\mu\text{-BL})]^{5+}$, which provides a means for examining changes in the IVCT characteristics whilst traversing the localised-to-delocalised transition.

In the present study, IVCT solvatochromism studies on the diastereoisomeric forms of $[\{Ru(bpy)_2\}_2(\mu\text{-BL})]^{5+}$ provide insights into the modification of solvent reorganisational effects (λ_o). In addition to the systematic electronic variations in the bridging ligands, the subtle structural and stereochemical variations within the series of complexes permit insights into spatially directed solvent interactions at the *molecular* level.

While the electrochemical, photochemical and photophysical properties of many of these complexes have been the subject of extensive research efforts over the past two decades,[21–25] the measurements have often been conducted without regard for the inherent stereoisomeric complexities,[17,18] and in many cases the theoretical implications of the results have been complicated by ion-pairing and ambiguities in the geometries of the complexes, due to a lack of structural rigidity and/or stereoisomeric purity.[17,18]

The redox and spectral properties for the diastereoisomeric forms of $[\{Ru(bpy)_2\}_2(\mu\text{-BL})]^{4+}$ (BL = dpb, dpb′),[14,26,27] and for diastereoisomeric mixtures of $[\{Ru(bpy)_2\}_2(\mu\text{-BL})]^{4+}$ (BL = dpb, dpq, and 2,3-dpp)[28–38] have been reported previously. However, their IVCT properties have received limited attention.[14,26,27] The bridging ligands possess unoccupied low-lying π^* orbitals and mediate electron transfer between the metal centres by means of a superexchange-assisted electron-transfer mechanism.[37] By the systematic variation in the energy of the lowest unoccupied molecular orbital (LUMO) of the bridging ligands, the change in the degree of electronic delocalisation (H_{ab}) on the IVCT properties may be assessed. The variations in the bridging ligands include the addition of electron-withdrawing phenyl groups fused to the side of the pyrazine ring through the two series.

Since the planarity of the bridging ligand influences its degree of electronic delocalisation, a comparison of the IVCT properties of the diastereoisomers of $[\{Ru(bpy)_2\}_2(\mu\text{-dpb}')]^{5+}$ and $[\{Ru(bpy)_2\}_2(\mu\text{-dpb})]^{5+}$ incorporating the "fused" and "unfused" bridging ligands provides insights into the influence of stereochemically induced structural distortions on the degree of delocalisation.

Results and Discussion

Diastereoisomer synthesis, separation and structural characterisation: The complexes $[\{Ru(bpy)_2\}_2(\mu\text{-BL})]^{4+}$ (BL = dpb′, dpq′, ppz, dpb, dpq and 2,3-dpp) were synthesised by the reaction of 2.2 equivalents of *cis*-$[Ru(bpy)_2Cl_2]\cdot 2H_2O$ with the bridging ligand in ethylene glycol, by using microwave-assisted methodology, which is well established for the synthesis of a range of dinuclear polypyridyl complexes of ruthenium.[14,19,26,27,39] This technique produced equivalent or increased reaction yields of the dinuclear species compared with previously reported thermal methods for the syntheses of $[\{Ru(bpy)_2\}_2(\mu\text{-BL})]^{4+}$ (BL = dpb,[30] ppz,[40,41] dpq and 2,3-dpp[28,31–35]). However, there was a significant reduction in the reaction times (typically from 2–24 h under the thermal refluxing procedure) to appoximately ten minutes under microwave-assisted conditions.

The separation of the diastereoisomeric forms of the dinuclear complexes was achieved by cation-exchange chromatography by using SP Sephadex C-25 as the support with aqueous solutions of sodium toluene-4-sulfonate as the eluent. In all cases, the band 1 and 2 eluates were determined to be the *meso* and *rac* diastereoisomers, respectively, from ^{1}H NMR characterisation and X-ray crystallography.

The assignments of the ^{1}H NMR spectra for the diastereoisomers of $[\{Ru(bpy)_2\}_2(\mu\text{-BL})]^{4+}$ (BL = dpb′, dpq′, ppz, dpb and 2,3-dpp) have been reported previously.[13,14,42] The ^{1}H numbering schemes for the diastereoisomers of $[\{Ru(bpy)_2\}_2(\mu\text{-dpq})]^{4+}$ are shown in Figure S1 in the Supporting

Information and the assignments of the spectra were performed with the assistance of ^{1}H COSY spectra and by comparison with the previously reported spectral assignments for $[\{Ru(bpy)_2\}_2(\mu\text{-BL})]^{4+}$. The coordinated bpy ligands exhibited the expected coupling constant values[43] ($J_{3,4}=8$ Hz, $J_{3,5}=1.5$ Hz, $J_{4,5}=8$ Hz, $J_{4,6}=1.5$ Hz and $J_{5,6}=5$ Hz) and coupling patterns based on the symmetry requirements of the complexes.

X-ray crystallography: The complex *rac*-(ΔΔ)-$[\{Ru(bpy)_2\}_2(\mu\text{-2,3-dpp})][PF_6]_4\cdot 4H_2O$ crystallised in the orthorhombic space group *Fdd2* with four dinuclear cations in the unit cell. A perspective view of the dinuclear cation is shown in Figure 2 and details of the crystal data and refinement are reported in Table S1 in the Supporting Information.

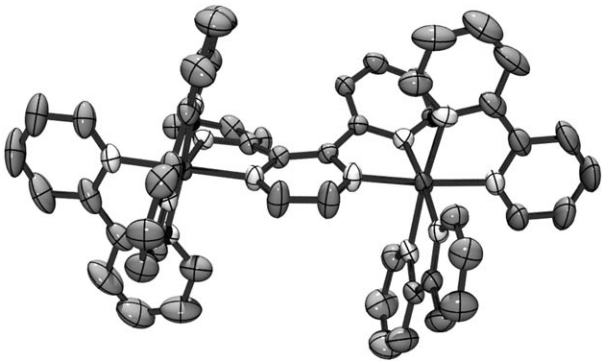

Figure 2. ORTEP plot of the X-ray crystal structure of the cation in *rac*-(ΔΔ)-$[\{Ru(bpy)_2\}_2(\mu\text{-2,3-dpp})][PF_6]_4\cdot 4H_2O$. Hydrogen atoms are omitted for clarity.

The crystal structure reveals a significant distortion of the bridging ligand, which is comparable to that observed previously for the dpb bridging ligand in *meso*-$[\{M(bpy)_2\}_2(\mu\text{-dpb})]^{4+}$ (M = Ru,[13,16] Os[16]). The 2,3-dpp ligand exhibits considerable distortion in the central pyrazine ring in addition to a large dihedral skew of the two pyridyl rings due to steric hindrance between the protons at the 3-position of the pyridyl rings. The metal centres reside in distorted octahedral environments and the average "bite-angles" subtended by the Ru centres and nitrogen atoms of the bridging ligand are 78.6(3)°. The Ru–N(pyrazine) and Ru–N(pyridine) bond lengths are 2.031(5) and 2.068(5) Å, respectively. The intermetal distance of 6.813(5) Å is consistent with the values reported previously for the complexes *meso*-$[\{Ru(bpy)_2\}_2(\mu\text{-BL})]^{4+}$ (BL = dpb, dpb′ and dpq′)[13] of 6.870(3), 6.887(1) and 6.818(1) Å, respectively.

At the present time a limited number of crystal structures of dinuclear ruthenium complexes containing bidentate polypyridyl terminal and bridging ligands have been reported in the literature.[44–50] The present report represents one of only a handful of structures that have been obtained through selective diastereoisomer isolation prior to crystal growth.[13,19,51–53]

Electrochemical and UV/Vis/NIR spectral characterisation: The redox potentials for the E_{ox1} ($[5^+/4^+]$; i.e., Ru^{III}–Ru^{II}/Ru^{II}–Ru^{II}) and E_{ox2} ($[6^+/5^+]$; i.e., Ru^{III}-Ru^{III}/Ru^{III}-Ru^{II}) couples for the series of complexes *meso*- and *rac*-$[\{Ru(bpy)_2\}_2(\mu\text{-BL})]^{4+}$ (BL = dpb′, dpq′, ppz, dpb, dpq and 2,3-dpp) were investigated by cyclic and differential pulse voltammetry in acetonitrile containing 0.1 M $[(n\text{-}C_4H_9)_4N]PF_6$, and are reported in Table 1. The reduction potentials are reported in Table S2 in the Supporting Information. Some details of the redox and spectral properties for the diastereoisomeric forms of $[\{Ru(bpy)_2\}_2(\mu\text{-BL})]^{4+}$ (BL = dpb, dpb′, dpq′, ppz),[13,14,26,27,42] and for diastereoisomeric mixtures of $[\{M(bpy)_2\}_2(\mu\text{-BL})]^{4+}$ (M = Os, Ru; BL = dpb, 2,3-dpp) have been reported previously.[28–38,54–56] The parameter ΔE_{ox} defines the potential difference between the $[6^+/5^+]$ and $[5^+/4^+]$ couples.

Table 1. Redox potentials for the oxidation processes [in mV relative to the Fc^+/Fc^0 couple] and K_c values[a] for the diastereoisomers of $[\{Ru(bpy)_2\}_2(\mu\text{-BL})]^{4+}$ in 0.1 M $[(n\text{-}C_4H_9)_4N]PF_6/CH_3CN$.[b]

BL	Diastereoisomer	K_c [$\times 10^{-3}$]	ΔE_{ox}	E_{ox2}	E_{ox1}
dpb′	*meso*	8.35	232	1300	1068
	rac	6.11	224	1304	1080
dpq′	*meso*	2.40	200	1285	1085
	rac	2.40	200	1297	1097
ppz	*meso*	6.11	224	1280	1056
	rac	4.48	216	1278	1062
dpb	*meso*	2.06	196	1280	1084
	rac	0.944	176	1280	1104
dpq	*meso*	1.80	192	1312	1120
	rac	1.12	180	1268	1088
2,3-dpp	*meso*	3.92	212	1256	1044
	rac	3.92	212	1244	1032

[a] K_c values are given by $K_c = \exp(\Delta E_{ox}F/RT)$, in which $F/RT = 38.92\ V^{-1}$ at 298 K.[57] [b] $\Delta E_{ox} = E_{ox2} - E_{ox1}$. Potentials are quoted ±3 mV.

The dinuclear systems are each characterised by two reversible one-electron redox processes corresponding to successive oxidation of the metal centres. There are multiple reversible ligand-based reductions in the cathodic region, for which the first two processes are assigned to the successive one-electron reductions of the bridging ligands ($BL^{0/-}$ and $BL^{-/2-}$), consistent with the stronger π-acceptor nature of the bridging ligand relative to the terminal bpy ligands.[28–38] The subsequent four one-electron processes correspond to successive reduction of the terminal bpy ligands and their potentials remain relatively constant with bridging ligand variation. In comparison, a cathodic shift of E_{red1} and E_{red2} is observed for the series of complexes that is consistent with the stabilisation of the π*(BL) LUMOs in the order ppz, dpq′, dpb′ for the fused bridging ligands, and 2,3-dpp, dpq, dpb for the unfused ligands. The parameters E_{red1} and E_{red2} are also shifted cathodically for the complexes that incorporate the unfused ligands, relative to their fused analogues.

Measurable differences in the ΔE_{ox} values are evident between the different complexes and between the diastereoisomeric forms of the same complex (with the exception of the

dpq′- and 2,3-dpp-bridged forms). The ΔE_{ox} values for the complexes incorporating the dpb and dpq bridging ligands were decreased relative to the other complexes in the series, and exhibited the largest differences between the values for the diastereoisomers of the same complex. The decrease in the ΔE_{ox} values for the diastereoisomers incorporating the unfused ligands relative to their fused counterparts and the significant difference in the values between the diastereoisomeric forms partly reflects the presence of structural distortions, which have been observed in the solid-state crystal structures of *meso*-$[\{Ru(bpy)_2\}_2(\mu\text{-dpb})]^{4+}$[13] and *rac*-$[\{Ru(bpy)_2\}_2(\mu\text{-2,3-dpp})]^{4+}$ (reported herein). However, these differences cannot be solely ascribed to variations in the extent of electronic delocalisation due to structural factors, as the magnitude of ΔE_{ox} also reflects contributions from ion-pairing interactions.[58] solvation energies and statistical factors.[56,59]

The UV/Vis/NIR spectral data for the unoxidised (+4), mixed-valence (+5) and fully-oxidised (+6) forms of $[\{Ru(bpy)_2\}_2(\mu\text{-BL})]^{n+}$ (BL = ppz, dpq′, dpb′, 2,3-dpp, dpb) over the range 3050–30000 cm^{-1} have been reported previously,[13,42] and the data for $[\{Ru(bpy)_2\}_2(\mu\text{-dpq})]^{4+}$ are reported in Table S3 in the Supporting Information. The spectra are characterised by a combination of overlapping $d\pi(Ru^{II}) \rightarrow \pi^*$(BL, bpy) singlet metal-to-ligand (^{1}MLCT) transitions. The lowest energy absorption band shifts to the red as BL is varied through the series ppz, dpq′, dpb′ for the fused bridging ligands, and 2,3-dpp, dpq, dpb for the unfused ligands, consistent with the increasing stabilisation of the π*(BL) orbitals for each series. The mixed-valence state was characterised by asymmetrically-shaped IVCT bands in the region 3500–9000 cm^{-1}.

Intervalence charge transfer (IVCT): The IVCT properties for the diastereoisomers of $[\{Ru(bpy)_2\}_2(\mu\text{-BL})]^{4+}$ (BL = dpb, dpb′, dpq′, ppz) in CH_3CN/0.1 M $[(n\text{-}C_4H_9)_4N]PF_6$ have been discussed previously.[13,16,42] In the present study, IVCT solvatochromism measurements on the diastereoisomers incorporating the full series of fused and unfused bridging ligands were performed at −35 °C in 0.02 M $[(n\text{-}C_4H_9)_4N][B(C_6F_5)_4]$ electrolyte[60] using a series of solvents including acetonitrile (CH_3CN, AN), propionitrile (CH_3CH_2CN, PN), *n*-butyronitrile ($CH_3(CH_2)_2CN$, BN), isobutyronitrile ($(CH_3)_2HCCN$, *i*BN), acetone ($(CH_3)_2CO$, AO) and dichloromethane (CH_2Cl_2, DCM). The solutions contained a uniform low concentration of the given diastereoisomer (0.40×10^{-3} M) to eliminate ion-pairing artefacts that are known to influence the IVCT characteristics.[13] An overlay of the IVCT bands for the full series of complexes in acetonitrile are shown in Figure 3, and the results of the band maxima (ν_{max}), molar absorption coefficients $\{(\varepsilon/\nu)_{max}\}$

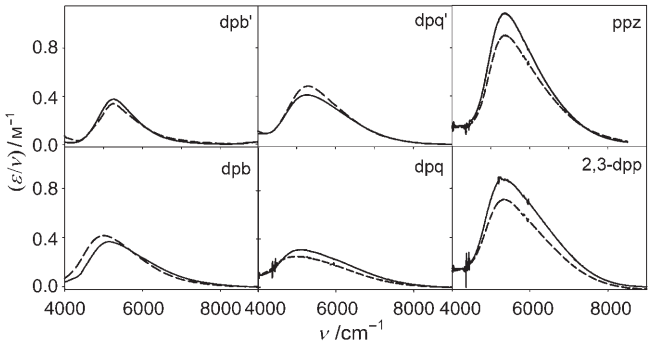

Figure 3. Overlay of the IVCT bands in CH_3CN for the *meso* (solid curves) and *rac* (dashed curves) $[\{Ru(bpy)_2\}_2(\mu\text{-BL})]^{5+}$ (BL = dpb, dpq, 2,3-dpp, dpb′, dpq′, ppz) in 0.02 M $[(n\text{-}C_4H_9)_4N][B(C_6F_5)_4]/CH_3CN$ at −35 °C.

and bandwidths ($\Delta\nu_{1/2}$) are summarised in Table 2. For all complexes, the bands are asymmetrically shaped and narrower on the lower energy side. A moment analysis of the IVCT bands was pursued,[1,61] and the results for the first-order moment analysis are also presented in Table 2, in which the zeroth- (M_0) and first-order (M_1) moments represent the band area and average band energy, respectively, and $|\mu_{12}|$ is the adiabatic transition moment. The electronic coupling parameters (H_{ab}) were determined from Equation (2),[62,63] in which e is the unit electronic charge and r_{ab} was assumed to be similar to the geometrical intermetal distance of 6.8 Å for all complexes.

$$H_{ab} = (|\mu_{12}|/e\,r_{ab})\nu_{max} \quad (2)$$

A classical two-state analysis[64] of the IVCT transitions

Table 2. IVCT spectral data of the reduced absorption spectra (ε/ν vs. ν) for the diastereoisomeric forms of $[\{Ru(bpy)_2\}_2(\mu\text{-BL})]^{5+}$ in 0.02 M $[(n\text{-}C_4H_9)_4N][B(C_6F_5)_4]/CH_3CN$ at −35 °C and parameters derived from the moment analysis of the transitions.[a]

BL	Diastereoisomer	ν_{max} [cm^{-1}]	$(\varepsilon/\nu)_{max}$ [M^{-1}]	$\Delta\nu_{1/2}$ [cm^{-1}]	M_0 [M^{-1}]	M_1 [cm^{-1}]	$\lvert\mu_{12}\rvert$ [e Å]	H_{ab} [cm^{-1}]	$\Delta\nu^o_{1/2}$ [cm^{-1}]
dpb	*meso*	5125	0.367	1718	688	5615	0.540	394	3070
	rac	4990	0.421	1634	753	5422	0.565	400	3026
dpq	*meso*	5092	0.312	2160	702	5344	0.531	398	3058
	rac	4948	0.253	2229	584	5384	0.496	360	3014
2,3-dpp	*meso*	5340	0.870	1812	1717	5152	0.806	632	3131
	rac	5340	0.707	1715	1349	5293	0.715	561	3131
dpb′	*meso*	5250	0.393	1048	482	5496	0.447	333	3105
	rac	5295	0.300	1250	460	5608	0.442	333	3118
dpq′	*meso*	5230	0.418	1755	802	5644	0.583	437	3100
	rac	5264	0.498	1566	871	5630	0.608	460	3110
ppz	*meso*	5356	1.084	1506	1892	5759	0.898	707	3136
	rac	5365	0.903	1566	1645	5500	0.836	660	3138

[a] The errors in the observed parameters are ±10 cm^{-1} for ν_{max}, M_1 and $\Delta\nu_{1/2}$; ±0.001 M^{-1} for $(\varepsilon/\nu)_{max}$; ±5 M^{-1} for M_0; and ±0.001 e Å for $|\mu_{12}|$.

reveals that all the systems exhibit significant electronic delocalisation. On the basis of the narrow bandwidths compared with the theoretical bandwidths ($\Delta\nu^{o}_{1/2}=[16RT\ln2(\lambda)]^{1/2}$, in which $16RT\ln2=1836\ cm^{-1}$ at 238 K), the systems lie close to the transition between the localised and delocalised regimes.

The data reveal significant differences in the IVCT characteristics not only between the different complexes, but also between the diastereoisomeric forms of the same complex. As the size of the "tail" of the bridging ligand increases through the series ppz, dpq′ and dpb′, and 2,3-dpp, dpq and dpb, the delocalisation of electron density over a larger area decreases the charge density at the Ru coordination sites. As a consequence, the values for M_0 (i.e., the band area) and the transition moment ($|\mu_{12}|$) decrease through each series of complexes. A corresponding trend in the magnitudes of H_{ab} is evident for the series ppz, dpq′ and dpb′, and to a lesser extent for the series 2,3-dpp, dpq and dpb. Similar trends were observed the full range of solvents employed. It should be noted that since the transfer of electron density decreases the *effective* electron-transfer distance relative to the diabatic distance (r_{ab}), the H_{ab} values shown in Table 2 represent lower limits only for the electronic-coupling parameter. A recent study re-evaluating the *effective* electron-transfer distance by Stark effect spectroscopy for the dpb′- and dpb-bridged complexes showed that the H_{ab} values required an upwards revision by a factor of at least three.[16]

While the IVCT energies (ν_{max}) were found to be identical within experimental error for both diastereoisomers of each complex incorporating ppz, dpq′, dpb′ and 2,3-dpp, the dpq- and dpb-bridged complexes exhibited a difference in energy of 144 and 135 cm^{-1}, respectively, between their diastereoisomers. These observations were consistent across the full series of solvents. The energy differences between the IVCT bands for the diastereoisomers incorporating unfused bridging ligands may be regarded as redox asymmetry contributions to the electron transfer barrier in Equation (1), and denoted by ΔE_{struct}.[15,16]

While structural distortions are likely to be present in the series of complexes incorporating the unfused bridging ligands, and are observed in the solid-state structures of *meso*-$[\{Ru(bpy)_2\}_2(\mu\text{-dpb})]^{4+}$[13] and *rac*-$[\{Ru(bpy)_2\}_2(\mu\text{-2,3-dpp})]^{4+}$, the extent of the differential distortion between the diastereoisomers may be expected to become increasingly more pronounced as the length of the "tail" of the bridging ligand is extended. By virtue of the greater extension of the benzoquinoxaline "tail" of the ligand, the distorted conformation of the bridge in this structure is maintained to a greater extent due to steric interactions between the hydrogen atoms on the long axis of the dpb bridge and the terminal bpy ligands, which are oriented differently in the two diastereoisomeric forms. Due to the smaller more compact nature of the 2,3-dpp bridging ligand, the extent of the differential distortion between the diastereoisomers is expected to be less pronounced than the dpb- and dpq-bridged complexes, and this is likely to account for the comparable values of the IVCT energies for the 2,3-dpp-bridged complex.

IVCT solvatochromism: The results for the IVCT characteristics as a function of $1/D_{op}-1/D_s$ are reported in Tables S4–S8 in the Supporting Information. Panels A and B in Figure 4 display overlays of the solvent dependence of ν_{max}, $\Delta\nu_{1/2}$ and M_1 for the complexes incorporating the fused and unfused bridging ligands, respectively.

In accordance with the dielectric continuum model [Eq. (3)], ν_{max} [Eq. (1)] should exhibit a linear dependence on $1/D_{op}-1/D_s$, with slope $e^2(1/a-1/d)$ and intercept $\lambda_i+\Delta E_0+\Delta E'$.[1,2] The parameters a and d define the molecular radii and distance between the donor and acceptor, and D_s and D_{op} are the static and optical dielectric constants of the solvent, respectively.

$$\lambda_o = e^2(1/a-1/d)(1/D_{op}-1/D_s) \quad (3)$$

In general, the IVCT parameters for the series of complexes exhibit a weak dependence on $1/D_{op}-1/D_s$, as shown in panels A and B of Figure 4; this dependence is consistent with charge-transfer transitions involving a minimal dipole moment change, a small residual barrier to intramolecular electron transfer and the classification of the complexes as borderline localised-to-delocalised systems.[6] Table S9 (in the Supporting Information) summarises the results for the slopes and intercepts of the solvatochromism plots of ν_{max} as a function of $1/D_{op}-1/D_s$.

Despite the weak solvent dependence of ν_{max}, differences are evident in the solvatochromism plots of M_1 as a function of $1/D_{op}-1/D_s$ between the different complexes, and between the diastereoisomeric forms of the same complex. The M_1 values are found to be relatively invariant to solvent for the dpb′- and dpb-bridged complexes, while the ppz- and 2,3-dpp-bridged complexes exhibit the steepest slopes, and hence the greatest solvent dependence. The solvent dependencies for the dpq′- and dpq-bridged complexes are intermediate between the two sets. Since the coordination geometries of the metal centres are identical for a given diastereoisomer across the series of complexes, the differences in IVCT solvatochromism properties arise from variations in the electronic and structural characteristics of the bridging ligands.

The trends in the solvent dependencies of ν_{max} and M_1 are mirrored in the plots of the $\Delta\nu_{1/2}$ as a function of $1/D_{op}-1/D_s$, shown in Figure 4. In general, the complexes incorporating the fused bridges exhibited narrower bandwidths and higher band energies than their unfused analogues, as shown in Figure S2 in the Supporting Information. The dpb′-bridged diastereoisomers exhibit the narrowest, solvent-independent bands, and the $\Delta\nu_{1/2}$ values for *rac*-$[\{Ru(bpy)_2\}_2(\mu\text{-dpb})]^{5+}$ are found to be solvent-independent, while a scattered variation in $\Delta\nu_{1/2}$ is evident for the *meso* form. The complexes incorporating the dpq′, ppz, dpq and 2,3-dpp bridging ligands exhibit an increase in $\Delta\nu_{1/2}$ with $1/D_{op}-1/D_s$, which is more pronounced for the unfused bridging ligands.

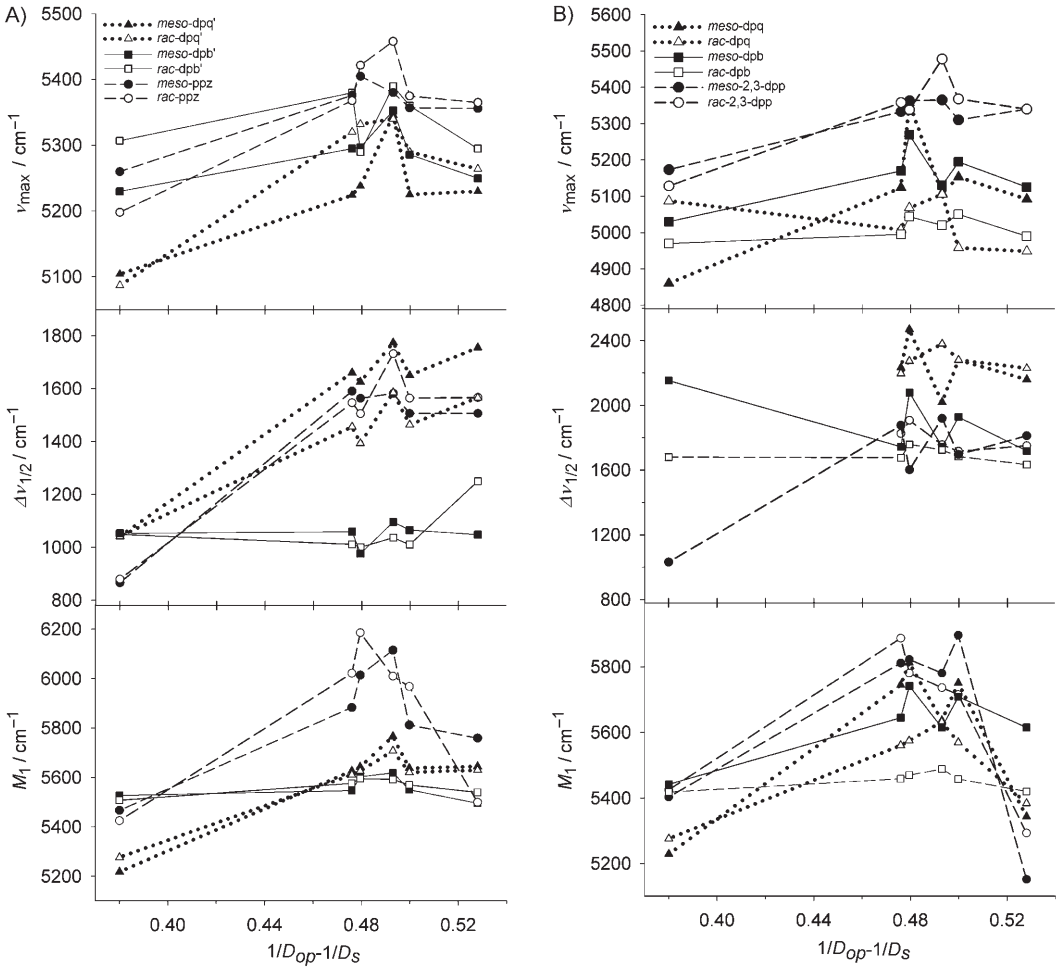

Figure 4. Solvent dependence of ν_{max}, $\Delta\nu_{1/2}$ and M_1 for the *meso* and *rac* diastereoisomers of $[\{Ru(bpy)_2\}_2(\mu\text{-BL})]^{5+}$ with A) BL = dpb′, dpq′, ppz and B) BL = dpb, dpq, 2,3-dpp in 0.02 M $[(n\text{-}C_4H_9)N][B(C_6F_5)_4]$/solvent at −35 °C. The $\Delta\nu_{1/2}$ values for *meso*-$[\{Ru(bpy)_2\}_2(\mu\text{-dpq})]^{5+}$ and *rac*-$[\{Ru(bpy)_2\}_2(\mu\text{-BL})]^{5+}$ (BL = dpq, 2,3-dpp) in dichloromethane could not be obtained reliably and are excluded. Error bars are omitted for clarity.

For both diastereoisomers of the dpb′-, ppz-, dpq- and 2,3-dpp-bridged complexes, the $\Delta\nu_{1/2}$ values were approximately identical across the series of solvents in each case, while the bandwidths for *meso*-$[\{Ru(bpy)_2\}_2(\mu\text{-dpq}')]^{5+}$ were consistently 200–300 cm^{-1} higher than the corresponding *rac* form.

From a classical approach,[1,2] the influence of the electronic coupling on the IVCT solvatochromism may be considered from two perspectives. Firstly, an increase in the electronic coupling decreases the effective charge-transfer distance relative to the geometrical distance. The results of the Stark effect measurements for *meso*-$[\{Ru(bpy)_2\}_2(\mu\text{-BL})]^{5+}$ (BL = dpb and dpq′)[16] revealed effective charge-transfer distances that were appreciably smaller than the geometrical metal–metal distances. This effect should be manifested by a decrease in the slope of the ν_{max} and M_1 solvatochromism plots due to the inverse dependence of λ_o on d at fixed d [Eq. (3)]. A similar explanation was proposed for the lower than expected solvent dependence of $[\{Ru(NH_3)_5\}_2(\mu\text{-4,4}'\text{-bpy})]^{5+}$.[65] Secondly, the influence of appreciable electronic delocalisation may be considered through the introduction of "effective amount of charge transfer", $(1-2b^2)e$, rather than e. The slope of the solvatochromism plot is given by $e^2(1/a-1/d)$ according to Equation (3); however, this equation is frequently expressed in terms of the effective amount of charge transferred, and the slope is given instead as $(\Delta e)^2(1/a-1/d)$. Since the effective amount of charge transferred is reduced from unit charge transfer by delocalisation, this explanation may provide a qualitative rationale for the decrease in the overall solvent dependence for the series of complexes incorporating the fused bridging ligands in the order ppz, dpq′ dpb′, and for the series incorporating the unfused bridging ligands in the order 2,3-dpp, dpq, dpb.

While electronic coupling effects provide a qualitative rationale for the weak solvent dependence of ν_{max} across the series of complexes, the trends in M_1 appear to signal a transition between the localised (class II) and localised-to-delocalised (class II–III) regimes.[6] The relatively strong solvent dependence for the ppz- and 2,3-dpp-bridged diastereoisomers indicates that these complexes lie in the class II region, and therefore exhibit localised oxidation states. The slight solvent-dependence of dpq′- and dpq-bridged diastereoisom-

ers indicates that these complexes also lie in the class II region, approaching class II–III, while the solvent-independent dpb′- and dpb-bridged complexes lie in the class II–III regime, in which the oxidation states are averaged. For the last two complexes, electron transfer occurs faster than solvent reorganisation and the solvent reorganisation is uncoupled from the electron transfer.

The trends in the bandwidths for the series of complexes support these classifications. For the fused bridging ligands, the broadening in the IVCT bands (in the full series of solvents) through the series dpb′ to dpq′ to ppz supports the increase in the degree of solvent coupling. The broader bandwidths for the complexes incorporating the unfused bridging ligands relative to their fused analogues can be rationalised primarily by the non-zero redox asymmetry contribution in the former case. The IVCT manifolds are composed of three underlying IVCT transitions that arise due to spin–orbit coupling and ligand-field asymmetry,[6] and we have recently demonstrated that the energy splitting between the components is increased due in the presence of structural distortions in *meso*- and *rac*-$[\{Ru(bpy)_2\}_2(\mu\text{-BL})]^{5+}$ (BL = dpb, 2,3-dpp).[16] On this basis, the increase in the $\Delta\nu_{1/2}$ values for the complexes incorporating the unfused bridging ligands relative to their fused counterparts can be rationalised primarily by the increase in the splitting of the three underlying components of the IVCT bands, rather than due to increased solvent coupling.

Stereochemically directed specific solvent effects: Specific solvation effects are reflected in the plots of the difference between the IVCT parameters for the diastereoisomers $\{\Delta\nu_{max}(meso\text{-}rac), \Delta(\Delta\nu_{1/2})(meso\text{-}rac)$ and $\Delta M_1(meso\text{-}rac)\}$ in panels A and B in Figure 5. These effects arise due to the penetration of solvent molecules within the *interior* clefts between the terminal bpy ligands, as the exterior clefts are identical for all diastereoisomers of the series of complexes. The plots of $\Delta\nu_{max}$ and ΔM_1 for the dpb′- and dpq′-bridged complexes exhibit similar trends across the series of solvents, as do the analogous unfused complexes incorporating the dpb and dpq bridging ligands. The magnitudes of $\Delta\nu_{max}$ and ΔM_1 are larger for the complexes incorporating the unfused ligands relative to their fused counterparts due to the inherent stereochemically induced redox asymmetry. It is likely that the specific interactions will couple to the solvent

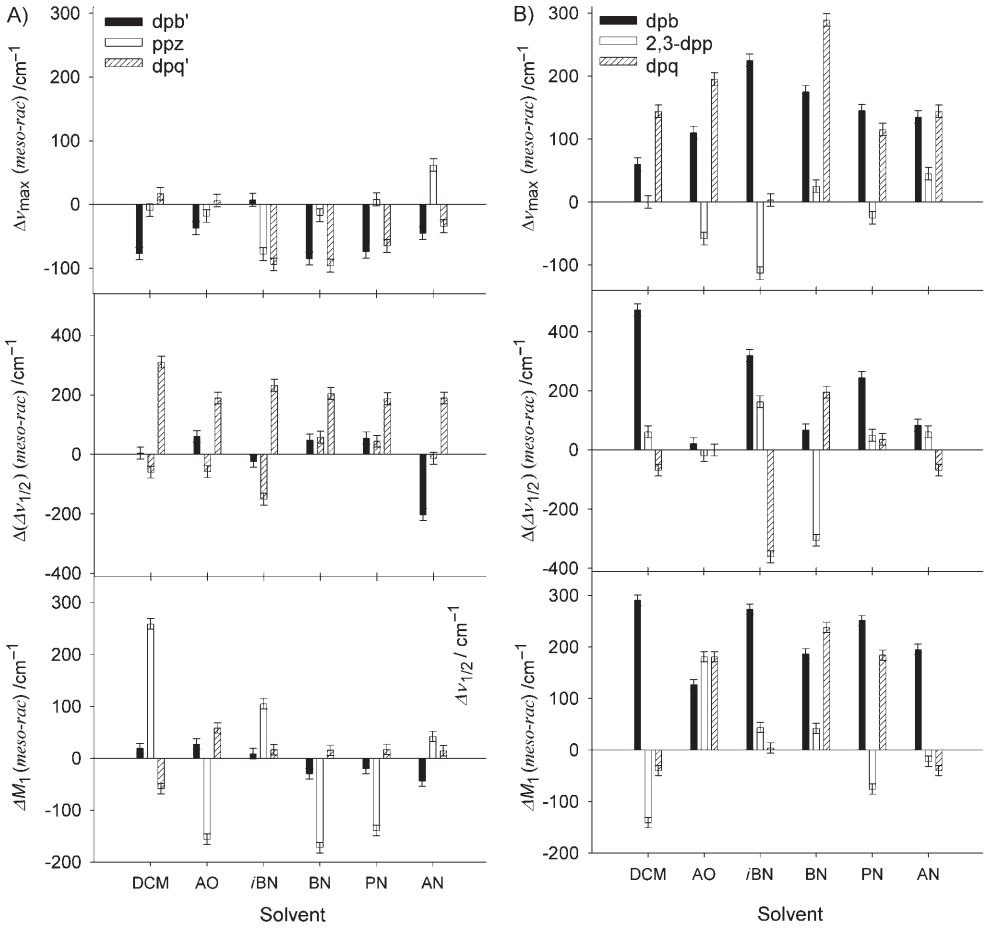

Figure 5. Differential energies, bandwidths and first moments of the IVCT transitions for the diastereoisomers of $[\{Ru(bpy)_2\}_2(\mu\text{-BL})]^{5+}$ with A) BL = dpb′, dpq′, ppz and B) BL = dpb, dpq, 2,3-dpp in 0.02 M $[(n\text{-}C_4H_9)N][B(C_6F_5)_4]$/solvent at −35 °C. The $\Delta\nu_{1/2}$ values for *meso*-$[\{Ru(bpy)_2\}_2(\mu\text{-dpq})]^{5+}$ and *rac*-$[\{Ru(bpy)_2\}_2(\mu\text{-BL})]^{5+}$ (BL = dpq, 2,3-dpp) in dichloromethane could not be obtained reliably and are excluded.

and electronic coordinates and invalidate the Franck–Condon approximation for this series of complexes.[8]

Predictions for the inner-sphere reorganisational barrier: According to the classical model,[1,2] the intercepts of the IVCT solvatochromism plots of ν_{max} as a function of $1/D_{op}-1/D_s$ given in Table S9 (see Supporting Information) provide estimates of the λ_i contributions in Equation (1). For the complexes incorporating the fused bridging ligands, the intercept is given by $\lambda_i+\Delta E'$ (since $\Delta E_0=0$), and for the series of complexes incorporating the unfused ligands by $\lambda_i+\Delta E'+\Delta E_{struct}$ (assuming that $\Delta E'$ and ΔE_{struct} are solvent-invariant). While the λ_i values for the three IVCT components may be extracted from Gaussian deconvolution of the IVCT manifolds, the errors in obtaining unique fits to the IVCT manifolds precluded such analyses. The parameter λ_i was therefore obtained from Equation (4),[66] in which Δ represents the energy difference between ν_{max} and the lowest energy component of the IVCT manifold, IVCT(1). Since the IVCT manifold consists of three IVCT transitions arising due to ligand-field and spin-orbit coupling, the first component {IVCT(1)} can be used to directly extract information about the mixed valence ground state.[6]

$$\nu_{max} = \lambda_i + \lambda_o + \Delta \quad (4)$$

Since the spin–orbit coupling constant for Ru (ξ_{Ru}) is known to be approximately one-third of that for Os (ξ_{Os}), an estimate of Δ for ruthenium complexes in the range 1750–1790 cm^{-1} has been obtained from the IC bands of analogous dinuclear osmium complexes (see Table S10 in the Supporting Information).[16] From Equation (4), λ_i can be estimated by subtracting the estimated value for Δ from the intercept of the ν_{max} versus $1/D_{op}-1/D_s$ plot (λ_o is zero as the intercept shows only solvent-independent contribution to ν_{max}). The intercepts for the complexes incorporating the fused and unfused bridging ligands were found to be within the ranges 4840–5475 and 3600–5185 cm^{-1}, respectively (Table S9 in the Supporting Information), which yields approximations for the value of λ_i as 3050–3725 cm^{-1} (fused) and 1810–3435 cm^{-1} (unfused). The larger range for λ_i in the latter case is consistent with the presence of a ΔE_{struct} term in expression for the intercept.

The significant magnitudes of λ_i are surprising in view of the small bond-length changes that occur upon oxidation of the complexes.[57,67] Estimates based on the Ru–N bond-length changes between $[Ru(bpy)_3]^{2+}$ and $[Ru(bpy)_3]^{3+}$ have led to an approximation of λ_i of less than 400 cm^{-1},[68] which is not compatible with the predicted values for λ_i in the present case. Such anomalies have been noted previously for related complexes such as $[\{Ru(bpy)_2(py)\}_2(\mu\text{-}4,4'\text{-}bpy)]^{5+}$,[69] in which the relatively large intercept of 6000 cm^{-1} was also difficult to rationalise from the small bond-length variations with oxidation.[57,67] The origin of the anomalous behaviour was attributed to delocalisation of the electron between the two sites, which invalidates the weak-coupling approximation that is implicit in Equation (3). In the present case, non-negligible electronic delocalisation [and so the invalidity of the localised assumption of Eq. (3)] may provide an explanation for the larger than expected λ_i values.

Conclusion

The systematic variation in the electronic properties of a series of di-bidentate bridging ligands in the complexes $[\{Ru(bpy)_2\}_2(\mu\text{-BL})]^{5+}$ has demonstrated the subtle influence of stereochemical and structural factors on the reorganisational energies (λ_o and λ_i) and the redox asymmetry (ΔE_0) contributions to the electron transfer barrier, as expressed in Equation (1). The consideration of the trends in the "raw" IVCT parameters (ν_{max}, $\Delta\nu_{1/2}$ and $(\varepsilon/\nu)_{max}$) in addition to the moments of the bands (M_0 and M_1), according to the dielectric continuum model, provides a qualitative basis for explaining the relative degree of coupling, with the allowance for stereochemically induced redox asymmetry and specific solvation effects.

IVCT solvatochromism studies on the diastereoisomers of $[\{Ru(bpy)_2\}_2(\mu\text{-BL})]^{5+}$ reveal that the solvent dependence of the IVCT parameters decreases through the series BL = ppz, dpq′, dpb′ (fused) and BL = 2,3-dpp, dpq, dpb (unfused). The trends are consistent with the increase in the degree of delocalisation as the "tails" of the bridging ligands are extended in each series. From a classical perspective, the solvent-independent systems bridged by dpb and dpb′ may be classified as class II–III systems, while the complexes incorporating ppz and 2,3-dpp exhibited the greatest solvent dependence, consistent with their class II classification. The solvent dependencies for the dpq- and dpq′-bridged diastereoisomers are intermediate between these two sets of complexes, in support of their classification as class II systems which lie at the borderline with the class II–III region. In general, the diastereoisomers of the complexes incorporating the unfused bridging ligands (2,3-dpp, dpq and dpb) exhibit more pronounced differences in their IVCT characteristics (over the full series of complexes) relative to their fused analogues due to the presence of a stereochemically induced redox asymmetry contribution.

The series of complexes $[\{Ru(bpy)_2\}_2(\mu\text{-BL})]^{4+}$ based on these bridging ligands have been investigated extensively over the past two decades as the basis of novel molecular materials capable of performing useful light- and/or redox-induced functions.[21–25] While these studies were performed without regard for the inherent stereochemistry of the systems, the present work demonstrates that stereochemical influences provide a significant contribution to the barrier to intramolecular electron transfer, and are indeed manifested in the electrochemical, spectral and IVCT properties. The realisation that metal–metal interactions in dinuclear polypyridyl complexes can be modified by the variation of their stereochemical properties has significant consequences for controlling such interactions in higher nuclearity polymetallic assemblies.

Experimental Section

Materials: Hydrated ruthenium trichloride ($RuCl_3 \cdot 3H_2O$; Strem, 99%), potassium hexafluorophosphate (KPF_6; Aldrich, 98%), lithium tetrakis-(pentafluorophenyl)borate ($Li[B(C_6F_5)_4] \cdot Et_2O$; Boulder Scientific), ethylene glycol (Ajax 95%), sodium toluene-4-sulfonate (Aldrich, 98%), DOWEX® 1×8, 50–100 mesh (Aldrich), Amberlite® IRA-400 (Aldrich) Cl^- ion exchange resins, Celite (Aldrich) and laboratory reagent solvents were used as received. Tetra-*n*-butylammonium hexafluorophosphate ($[(n\text{-}C_4H_9)_4N]PF_6$; Fluka, 99+%) was dried in vacuo at 60°C and ferrocene (Fc; BDH) was purified by sublimation prior to use. SP Sephadex C-25, Sephadex LH-20 (Amersham Pharmacia Biotech), and silica gel (200–400 mesh , 60 Å, Aldrich) were employed for the chromatographic separation and purification of ruthenium complexes.[17] Prior to use, acetonitrile (CH_3CN; Aldrich, 99.9+%) and propionitrile (PN; Aldrich) were distilled over CaH_2, while acetone (BDH, HPLC grade) was distilled over K_2CO_3 and dichloromethane over $CaCl_2$. *n*-Butyronitrile (BN; Aldrich, 99+%), isobutyronitrile (*i*BN; Aldrich), and benzonitrile (BzN; Aldrich) were used as received. $[(n\text{-}C_4H_9)_4N][B(C_6F_5)_4]$[60] was prepared by metathesis from $Li[B(C_6F_5)_4] \cdot Et_2O$ as described previously.[12] The bridging ligand dpq was supplied by Dr Laurence Kelso and was prepared according to the literature methodology.[70]

General: 1D and 2D ^1H NMR spectra were collected on a Varian Mercury 300 MHz spectrometer. ^1H NMR chemical shifts for all complexes are reported relative to 99.9% [D_3]acetonitrile (CD_3CN; Cambridge Isotope Laboratories (CIL)) at $\delta = 1.93$ ppm. ^1H NMR assignments were performed with the assistance of COSY experiments to identify each pyridine ring system. Elemental microanalyses were performed at the Microanalytical Unit in the Research School of Chemistry, Australian National University. An allowance for hydration was necessary to account for analysis figures within the acceptable limits (±0.4%).

Electrochemistry: Electrochemical measurements were performed under argon by using a Bioanalytical Systems (BAS) 100 A Electrochemical Analyser. Cyclic (CV) and differential pulse (DPV) voltammograms were recorded in a standard three-electrode cell using a glassy carbon or platinum button working electrode, a platinum wire auxiliary electrode and an Ag/AgCl reference electrode (0.1 M $[(n\text{-}C_4H_9)_4N]PF_6$ in CH_3CN). Ferrocene was added as an internal standard on completion of each experiment (the ferrocene/ferrocenium couple (Fc^+/Fc^0) occurred at +550 mV versus Ag/AgCl). Solutions contained 0.1 M $[(n\text{-}C_4H_9)_4N]PF_6$ as electrolyte. Cyclic voltammetry was performed with a sweep rate of 100 mV s^{-1}; differential pulse voltammetry was conducted with a sweep rate of 4 mV s^{-1} and a pulse amplitude, width and period of 50 mV, 60 ms and 1 s, respectively. All potentials are reported ±3 mV.

UV/Vis/NIR spectroelectrochemistry: UV/Vis/NIR spectroelectrochemistry was performed by using a CARY 5E spectrophotometer interfaced to Varian WinUV software. The absorption spectra of the electrogenerated mixed-valence species were obtained in situ by the use of a cryostatted optically semitransparent thin-layer electrosynthetic (OSTLE) cell.[71] An account of the procedure employed in the spectroelectrochemical measurements has been detailed previously.[72] Solutions for the spectroelectrochemial experiments contained 0.02 M $[(n\text{-}C_4H_9)_4N][B(C_6F_5)_4]$ supporting electrolyte in CH_3CN and the complex (ca. 0.4×10^{-3} M). The temperature was stabilised to ±0.3°C prior to commencing electrolysis. The dinuclear systems required approximately 6 h for data collection at −35°C.

The analysis and spectral deconvolution of the data were performed as described in a previous report.[13] The IVCT spectra were scaled as $\int \varepsilon(\nu)/\nu \, d\nu$[1,61] and deconvolution of the NIR transitions was performed by using the curve-fitting subroutine implemented within the GRAMS32 commercial software package, as described previously.[72] Based on the reproducibility of the parameters obtained from the deconvolutions, the uncertainties in the energies (ν_{max}), intensities $\{(\varepsilon/\nu)_{max}\}$ and bandwidths ($\Delta\nu_{1/2}$) were estimated as ±10 cm^{-1}, ±0.001 M^{-1} cm^{-1} and ±10 cm^{-1}, respectively.

For asymmetrically shaped IVCT bands, an examination of the moments of the band is required, rather than the experimentally observed quantities (ν_{max}, $\Delta\nu_{1/2}$ and $(\varepsilon/\nu)_{max}$). The first-order moment (M_1) defines the average energy of the absorption manifold and is given by Equation (5).[1] The parameter $f(\nu)$ is the line-shape function of the reduced absorption spectrum $\{(\varepsilon/\nu)$ vs. $\nu\}$. The denominator represents the area under the band of the reduced absorption spectrum, that is, the zeroth-moment M_0 [Eq. (6)]. The transition moment ($|\mu_{12}|$ in e Å) is defined as 0.0206 Å × $M_0^{1/2}$.

$$M_1 = \frac{1}{M_0} \int_{\nu 1}^{\nu 2} \nu f(\nu) \, d\nu \tag{5}$$

$$M_0 = \int_{\nu 1}^{\nu 2} f(\nu) \, d\nu \tag{6}$$

Synthesis of dinuclear complexes and separation of diastereoisomers: A detailed account of the microwave techniques and column chromatographic procedures employed for the separation and purification of the diastereoisomers is provided has been reported previously.[19] $[Ru(bpy)_2Cl_2] \cdot 2H_2O$,[73] $[\{Ru(bpy)_2\}_2(\mu\text{-dpb})][PF_6]_4$,[13,14,26] $[\{Ru(bpy)_2\}_2(\mu\text{-2,3-dpp})][PF_6]_4$,[16] $[\{Ru(bpy)_2\}_2(\mu\text{-dpb}')][PF_6]_4$,[14] $[\{Ru(bpy)_2\}_2(\mu\text{-dpq}')][PF_6]_4$[13] and $[\{Ru(bpy)_2\}_2(\mu\text{-ppz})][PF_6]_4$[42] were prepared according to the previously reported methods.

$[\{Ru(bpy)_2\}_2(\mu\text{-dpq})][PF_6]_4 \cdot 5H_2O$: A suspension of dpq (55 mg, 0.192 mmol) and *cis*-$[Ru(bpy)_2Cl_2] \cdot 2H_2O$ (200 mg, 0.384 mmol) in ethylene glycol (3 cm^3) was heated at reflux in a modified microwave oven (Sharp, Model R-2 V55; 600 W, 2450 MHz) on medium high power for 3×3 mins during which time the solution attained a dark green colouration. The mixture was diluted in water (ca. 40 cm^3) and the dinuclear product was separated from the crude mixture via a gradient elution procedure using aqueous 0.1–0.5 M NaCl as the eluent. A claret-red band of mononuclear material eluted first (0.3 M NaCl) followed by the desired dark green product (0.6 M NaCl) which was precipitated as the PF_6^- salt by addition of a saturated solution of aqueous KPF_6. The solid was isolated by vacuum filtration and washed with diethyl ether (3×10 cm^3). Yield: 198 mg (61%). Elemental analysis calcd (%) for $C_{58}H_{54}F_{24}N_{12}O_5P_4Ru_2$: C 39.11, H 3.00, N 9.44; found: C 39.08, H 2.61, N 9.12.

Separation of the diastereoisomers was achieved by cation exchange chromatography on SP Sephadex C-25 support (dimensions 96 cm length × 1.6 cm diameter). The complex (ca. 80 mg) was loaded onto the column in aqueous solution (as the Cl^- form, obtained by stirring an aqueous suspension of the complex with Amberlite® anion exchange resin) and eluted with 0.25 M sodium toluene-4-sulfonate solution.[19] The diastereoisomers separated after passing through an effective column length of 3 m. The two bands were collected, saturated aqueous KPF_6 solution added and the products extracted with dichloromethane. The organic extracts were dried with anhydrous Na_2SO_4 and the solvent removed by rotary evaporation.

Rigorous purification methods were employed prior to characterisation and physical measurements due to the potentially strong associations between the complex cations and the anions present in the eluents employed in the chromatographic separations.[19,20] Each product was dissolved in a minimum volume of acetone and loaded onto a short column of silica gel (dimensions 3×2.5 cm), washed with acetone, water and acetone and eluted with acetone containing 5% NH_4PF_6. Addition of water and removal of the acetone under reduced pressure afforded dark green solids, which were collected by filtration through Celite and washed with diethyl ether (3×5 cm^3). Bands 1 and 2 were determined to be the *meso* and *rac* diastereoisomers, respectively, as established by X-ray crystallography and NMR characterisation.

Band 1 (*meso*): ^1H NMR (CD_3CN): $\delta = 6.69$ (dd, $J = 5.8$, 0.6 Hz, 1H), 7.10 (dd, $J = 8.7$, 0.6 Hz, 1H), 7.23 (d, $J = 7.9$ Hz, 1H), 7.27 (d, $J = 4.7$ Hz, 1H), 7.35 (t, $J = 8.8$ Hz, 2H), 7.36–7.49 (m, 10H), 7.59 (t, $J = 7.1$ Hz, 1H), 7.64 (t, $J = 5.8$ Hz, 1H), 7.70 (d, $J = 4.6$ Hz, 1H), 7.78 (dd, $J = 5.6$, 1.3 Hz, 1H), 7.83 (td, $J = 8.1$, 1.3 Hz, 1H), 7.87–8.25 (m, 16H), 8.31 (dd, $J = 8.3$, 0.6 Hz, 1H), 8.36 (dd, $J = 5.5$, 0.9 Hz, 1H), 8.43 (dd, $J = 7.7$, 0.6 Hz, 1H), 8.49 (dd, $J = 7.8$, 0.6 Hz, 1H), 8.56 (td, $J = 9.0$, 0.6 Hz, 2H), 8.72 (dd, $J = 5.7$,

0.9 Hz, 1H), 8.75 (dd, $J=5.8$, 0.7 Hz, 1H), 8.82 ppm (dd, $J=8.1$, 0.6 Hz, 1H).

Band 2 (*rac*): ^{1}H NMR (CD_3CN): $\delta=7.19$ (td, $J=6.1$, 1.0 Hz, 2H), 7.36–7.54 (m, 12H), 7.57 (dd, $J=5.3$, 1.0 Hz, 2H), 7.62 (td, $J=6.1$, 1.0 Hz, 2H), 7.75 (d, $J=4.1$ Hz, 2H), 7.76 (d, $J=4.2$ Hz, 2H), 7.85 (dd, $J=5.6$, 1.0 Hz, 2H), 7.98–8.10 (m, 6H), 8.14 (td, $J=7.9$, 1.5 Hz, 2H), 8.18 (td, $J=7.9$, 1.2 Hz, 2H), 8.23 (d, $J=5.4$ Hz, 2H), 8.34 (d, $J=8.3$ Hz, 4H), 8.68 (d, $J=8.2$ Hz, 4H), 8.74 ppm (d, $J=8.1$ Hz, 2H). The ^{1}H NMR numbering scheme is shown in Figure S1 (in the Supporting Information). Complete spectral assignments were not possible due to the convoluted nature of the 1D and 2D spectra.

X-ray crystallography: Single crystals of *rac*-$[\{Ru(bpy)_2\}_2(\mu\text{-}2,3\text{-}dpp)][PF_6]_4\cdot 4H_2O$ were grown by slow evaporation of a solution of about 1 mmol of the complex in acetone/water (2:1 ca. 1 mL) under ambient conditions in the absence of light. The collection and refinement of X-ray data was performed in the Advanced Analytical Centre at James Cook University. Hemispheres of data were collected (on crystals coated with polyacrylamide glue) at −50 °C on a Bruker SMART CCD diffractometer using the omega scan mode. A summary of the data collection and refinement details is provided in Table S1 in the Supporting Information. Data sets were corrected for absorption using the program SADABS.[74] The solution and refinement for all structures was carried out by using SHELXL-97[75] utilising the graphical interface WinGX.[76] CCDC-291106 contains the supplementary crystallographic data for this paper. These data can be obtained free of charge from The Cambridge Crystallographic Data Centre via www.ccdc.cam.ac.uk/data_request/cif.

Acknowledgements

We gratefully acknowledge the financial support of the Australian Research Council.

[1] N. S. Hush, *Prog. Inorg. Chem.* **1967**, *8*, 391–444.
[2] N. S. Hush, *Electrochim. Acta* **1968**, *13*, 1005–1023.
[3] R. A. Marcus, *J. Chem. Phys.* **1957**, *26*, 867–871.
[4] R. A. Marcus, *J. Chem. Phys.* **1956**, *24*, 966–978.
[5] M. B. Robin, P. Day, *Adv. Inorg. Chem. Radiochem.* **1967**, *10*, 247–403.
[6] K. D. Demadis, C. M. Hartshorn, T. J. Meyer, *Chem. Rev.* **2001**, *101*, 2655–2685.
[7] B. S. Brunschwig, C. Creutz, N. Sutin, *Chem. Soc. Rev.* **2002**, *31*, 168–184.
[8] P. Chen, T. J. Meyer, *Chem. Rev.* **1998**, *98*, 1439–1477.
[9] S. F. Nelsen, *Chem. Eur. J.* **2000**, *6*, 581–588.
[10] P. F. Barbara, T. J. Meyer, M. A. Ratner, *J. Phys. Chem.* **1996**, *100*, 13148–13168.
[11] J. R. Reimers, N. S. Hush, *Chem. Phys.* **1996**, *208*, 177–193.
[12] D. M. D'Alessandro, F. R. Keene, *Chem. Phys.* DOI: 10.1016/j.chemphys.2005.09.016.
[13] D. M. D'Alessandro, P. C. Junk, F. R. Keene, *Supramol. Chem.* **2005**, *17*, 529–542.
[14] D. M. D'Alessandro, L. S. Kelso, F. R. Keene, *Inorg. Chem.* **2001**, *40*, 6841–6844.
[15] D. M. D'Alessandro, F. R. Keene, *Aust. J. Chem.* **2005**, *58*, 767–777.
[16] D. M. D'Alessandro, P. H. Dinolfo, M. S. Davies, J. T. Hupp, F. R. Keene, *Inorg. Chem.* DOI: 10.1021/ic051841f.
[17] F. R. Keene, *Chem. Soc. Rev.* **1998**, *27*, 185–193.
[18] F. R. Keene, *Coord. Chem. Rev.* **1997**, *166*, 122–159.
[19] N. C. Fletcher, P. C. Junk, D. A. Reitsma, F. R. Keene, *J. Chem. Soc. Dalton Trans.* **1998**, 133–138.
[20] N. C. Fletcher, F. R. Keene, *J. Chem. Soc. Dalton Trans.* **1999**, 683–689.
[21] C. G. Garcia, J. F. de Lima, N. Y. M. Iha, *Coord. Chem. Rev.* **2000**, *196*, 219–247.
[22] P. Belser, S. Bernhard, C. Blum, A. Beyeler, L. De Cola, V. Balzani, *Coord. Chem. Rev.* **1999**, *190–192*, 155–169.
[23] V. Balzani, A. Juris, M. Venturi, S. Campagna, S. Serroni, *Chem. Rev.* **1996**, *96*, 759–833.
[24] P. Belser, R. Dux, M. Baak, L. De Cola, V. Balzani, *Angew. Chem.* **1995**, *107*, 634–637; *Angew. Chem. Int. Ed. Engl.* **1995**, *34*, 595–598.
[25] V. Balzani, F. Scandola, *Supramolecular Photochemistry*, Horwood, Chichester (UK), **1991**.
[26] B. D. Yeomans, L. S. Kelso, P. A. Tregloan, F. R. Keene, *Eur. J. Inorg. Chem.* **2001**, 239–246.
[27] L. S. Kelso, Ph.D. thesis, James Cook University, Townsville, Australia, **2000**.
[28] G. Denti, S. Campagna, L. Sabatino, S. Serroni, M. Ciano, V. Balzani, *Inorg. Chem.* **1990**, *29*, 4750–4758.
[29] D. S. Seneviratne, M. J. Uddin, V. Swayambunathan, H. B. Schlegel, J. F. Endicott, *Inorg. Chem.* **2002**, *41*, 1502–1517.
[30] S. M. Molnar, K. R. Neville, G. E. Jensen, K. J. Brewer, *Inorg. Chim. Acta* **1993**, *206*, 69–76.
[31] A. W. Wallace, W. R. Murphy, J. D. Petersen, *Inorg. Chim. Acta* **1989**, *166*, 47–54.
[32] S. M. Scott, K. C. Gordon, *Inorg. Chim. Acta* **1997**, *254*, 267–272.
[33] J. E. B. Johnson, R. R. Ruminski, *Inorg. Chim. Acta* **1993**, *208*, 231–237.
[34] C. H. Braunstein, A. D. Baker, T. C. Strekas, H. D. Gafney, *Inorg. Chem.* **1984**, *23*, 857–864.
[35] P. Rillema, K. B. Mack, *Inorg. Chem.* **1982**, *21*, 3849–3854.
[36] R. M. Berger, *Inorg. Chem.* **1990**, *29*, 1920–1924.
[37] G. Giuffrida, S. Campagna, *Coord. Chem. Rev.* **1994**, *135*, 517–531.
[38] A. Juris, S. Barigelletti, S. Campagna, V. Balzani, P. Belser, A. von Zelewsky, *Coord. Chem. Rev.* **1988**, *84*, 85–277.
[39] T. J. Rutherford, O. Van Gijte, A. Kirsch-De Mesmaeker, F. R. Keene, *Inorg. Chem.* **1997**, *36*, 4465–4474.
[40] Y. Fuchs, S. Lofters, T. Dieter, W. Shi, T. C. Morgan, T. C. Strekas, H. D. Gafney, A. D. Baker, *J. Am. Chem. Soc.* **1987**, *109*, 2691–2697.
[41] O. Morgan, S. Wang, S.-A. Bae, R. J. Morgan, A. D. Baker, T. C. Strekas, R. Engel, *J. Chem. Soc. Dalton Trans.* **1997**, 3773–3776.
[42] D. M. D'Alessandro, F. R. Keene, *Dalton Trans.* **2006**, 1060–1072.
[43] E. C. Constable, J. Lewis, *Inorg. Chim. Acta* **1983**, *70*, 251–253.
[44] H. Masui, A. L. Freda, M. C. Zerner, A. B. P. Lever, *Inorg. Chem.* **2000**, *39*, 141–152.
[45] S. D. Bergman, I. Goldberg, A. Barbieri, F. Barigelletti, M. Kol, *Inorg. Chem.* **2004**, *43*, 2355–2367.
[46] D. Bardwell, J. C. Jeffery, L. Joulie, M. D. Ward, *J. Chem. Soc. Dalton Trans.* **1993**, 2255–2256.
[47] D. A. Bardwell, L. Horsburgh, J. C. Jeffery, L. F. Joulié, M. D. Ward, I. Webster, L. J. Yellowlees, *J. Chem. Soc. Dalton Trans.* **1996**, 2527–2531.
[48] R. Hage, J. G. Haasnoot, H. A. Nieuwenhuis, J. Reedijk, D. J. A. De Ridder, J. G. Vos, *J. Am. Chem. Soc.* **1990**, *112*, 9245–9251.
[49] V. Balzani, D. A. Bardwell, F. Barigelletti, F. L. Cleary, M. Guardigli, J. C. Jeffery, T. Sovrani, M. D. Ward, *J. Chem. Soc. Dalton Trans.* **1995**, 3601–3608.
[50] D. Gut, I. Goldberg, M. Kol, *Inorg. Chem.* **2003**, *42*, 3483–3491.
[51] C. Richardson, P. J. Steel, D. M. D'Alessandro, P. C. Junk, F. R. Keene, *J. Chem. Soc. Dalton Trans.* **2002**, 2775–2785.
[52] J. A. Zampese, F. R. Keene, P. J. Steel, *Dalton Trans.* **2004**, 4124–4129.
[53] D. M. D'Alessandro, F. M. Foley, M. S. Davies, P. C. Junk, F. R. Keene, *Polyhedron*, in press.
[54] M. M. Richter, K. J. Brewer, *Inorg. Chim. Acta* **1991**, *180*, 125–131.
[55] M. M. Richter, K. J. Brewer, *Inorg. Chem.* **1993**, *32*, 2827–2834.
[56] K. A. Goldsby, T. J. Meyer, *Inorg. Chem.* **1984**, *23*, 3002–3010.
[57] C. Creutz, *Prog. Inorg. Chem.* **1983**, *30*, 1–73.
[58] D. M. D'Alessandro, F. R. Keene, *Dalton Trans.* **2004**, 3950–3954.
[59] D. E. Richardson, H. Taube, *J. Am. Chem. Soc.* **1983**, *105*, 40–51.
[60] R. LeSuer, W. E. Geiger, *Angew. Chem.* **2000**, *112*, 254–256; *Angew. Chem. Int. Ed.* **2000**, *39*, 248–250.
[61] J. R. Reimers, N. S. Hush, *Inorg. Chem.* **1990**, *29*, 3686–3697.

[62] C. Creutz, M. D. Newton, N. Sutin, *J. Photochem. Photobiol. A* **1994**, *82*, 47–59.
[63] R. J. Cave, M. D. Newton, *Chem. Phys. Lett.* **1996**, *249*, 15–19.
[64] N. S. Hush, *Coord. Chem. Rev.* **1985**, *64*, 135–157.
[65] J. T. Hupp, Y. H. Dong, R. L. Blackbourn, H. Lu, *J. Phys. Chem.* **1993**, *97*, 3278–3282.
[66] J. T. Hupp, T. J. Meyer, *Inorg. Chem.* **1987**, *26*, 2332–2334.
[67] C. Creutz, *Inorg. Chem.* **1978**, *17*, 3723–3725.
[68] B. S. Brunschwig, C. Creutz, D. H. Macartney, T.-K. Sham, N. Sutin, *Faraday Discuss. Chem. Soc.* **1982**, *74*, 113–127.
[69] M. J. Powers, T. J. Meyer, *Inorg. Chem.* **1978**, *17*, 1785–1790.
[70] S. Kasselouri, A. Garoufis, A. Katehanakis, G. Kalkanis, S. P. Perlepes, N. Hadjiliadis, *Inorg. Chim. Acta* **1993**, *20*, 255–258.
[71] C. M. Duff, G. A. Heath, *Inorg. Chem.* **1991**, *30*, 2528–2535.
[72] D. M. D'Alessandro, F. R. Keene, *Chem. Eur. J.* **2005**, *11*, 3679–3688.
[73] T. Togano, N. Nagao, M. Tsuchida, H. Kumakura, K. Hisamatsu, F. S. Howell, M. Mukaida, *Inorg. Chim. Acta* **1992**, *195*, 221–225.
[74] R. H. Blessing, *Acta. Crystallogr Sect. A* **1995**, *51*, 33–38.
[75] G. M. Sheldrick, SHELX97, Programs for Crystal Structure Analysis, Institüt für Anorganische Chemie der Universitat Gottingen, Gottingen, **1997**.
[76] L. J. Farrugia, *J. Appl. Crystallogr.* **1999**, *32*, 837–838.

Received: November 30, 2005
Published online: April 5, 2006

